An Interactive Three Dimensional approach to Anatomical Description – The jaw musculature of the Australian Laughing Kookaburra (*Dacelo novaeguineae*)

The investigation of form-function relationships requires a detailed understanding of anatomical systems. Here we document the 3-dimensional morphology of the cranial musculoskeletal anatomy in the Australian Laughing Kookaburra *Dacelo novaeguineae*, with a focus upon the geometry and attachments of the jaw muscles in this species. The head of a deceased specimen was CT scanned, and an accurate 3D representation of the skull and jaw muscles was generated through manual segmentation of the CT scan images, and augmented by dissection of the specimen. We identified 14 major jaw muscles: 6 in the temporal group (*M. adductor mandibulae* and *M. pseudotemporalis*), 7 in the pterygoid group (*M. pterygoideus dorsalis* and *M. pterygoideus ventralis*), and the single jaw abductor *M. depressor mandibulae*. Previous descriptions of avian jaw musculature are hindered by limited visual representation and inconsistency in the nomenclature. To address these issues, we: (1) present the 3D model produced from the segmentation process as a digital, fully interactive model in the form of an embedded 3D image, which can viewed from any angle, and within which major components can be set as opaque, transparent, or hidden, allowing the anatomy to be visualised as required to provide a detailed understanding of the jaw anatomy; (2) provide a summary of the nomenclature used throughout the avian jaw muscle literature. The approach presented here provides considerable advantages for the documentation and communication of detailed anatomical structures in a wide range of taxa.

1   Michelle R Quayle[1], David G Barnes[2,3,4], Owen L Kaluza[5], Colin R McHenry[1]

2   [1] Department of Anatomy and Developmental Biology, School of Biomedical Sciences, Monash
3   University, Clayton, VIC 3800, Australia
4   [2] Monash Biomedical Imaging, Monash University, Clayton, VIC 3800, Australia
5   [3] VLSCI Life Sciences Computation Centre, Carlton, VIC 3010, Australia
6   [4] Clayton School of Information Technology, Monash University, Clayton, VIC 3800, Australia
7   [5] Monash e-Research Centre, Monash University, Clayton, VIC 3800, Australia

8   **Introduction**

9   The relationship between form and function is a central concept in biology (Lauder et al., 1995;
10   Russell 1916; Thompson 1916); it determines the extent to which the anatomy of an organism
11   permits specific behaviours and ecology. Investigating form-function relationships requires a
12   detailed understanding of anatomical systems, i.e. the discipline of anatomy and morphology. For
13   functional questions concerning feeding ecology, the relevant anatomical system is the feeding
14   apparatus; for the majority of vertebrates, this consists of the jaws. The jaw is a functional unit,
15   consisting of a rigid framework – the skull bones of the cranium and mandible, operated by a
16   system of jaw muscles. The skull bones must be able to withstand the forces of catching a
17   struggling prey item, whilst transferring the bite force generated from the jaw muscles to hold,
18   kill and process the prey without sustaining fracture. Fundamentally, the mechanical limits of the
19   jaw's ability to bite the prey item determines the type and size of prey that can be taken (Ferrara
20   et al., 2011; Herrel et al., 2002; Wroe et al., 2005).

22   Form-function relationships can be investigated using mechanistic techniques, such as
23   computational biomechanics, and/or quantitative approaches, such as statistics and
24   morphometrics. For biomechanical modelling, the jaw musculature is an important component of
25   the loads that act upon the skull during feeding and other behaviours. During biting, **isotonic**
26   contraction of the adductor musculature imposes reaction forces on the prey (or other item),
27   whilst shaking or twisting of the food requires **isometric** contraction of the jaw muscles to firmly
28   hold the prey. During each of these activities, the activation of the jaw musculature imposes
29   tensile forces to attachment areas which can result in loads at least as high as the loads being
30   applied to the prey (Herring et al., 2001). Therefore, to simulate the jaw as closely to the actual
31   system as possible it is important to include an accurate representation of the jaw musculature in
32   the model.

33

34   The following description of the jaw musculature of the Australian laughing kookaburra (*Dacelo*
35   *novaeguineae*) was stimulated by the need to incorporate detailed anatomical data into high
36   resolution 3D finite element models as part of an analysis of skull biomechanics in 8 species of
37   kingfisher (Alcedines) (Quayle 2011; Quayle et al., in prep.). *Dacelo novaeguineae* was chosen

38 as a representative species of kingfisher for anatomical description as it is common species in our
39 location meaning that specimens are readily available and it has a large body size compared to
40 other species of kingfishers; allowing for the small jaw muscles to be more easily detectable
41 through imaging and dissection techniques. This is the first time that the jaw musculature of this
42 species has been documented.

43 **Avian and kingfisher cranial anatomy**
44 A review of the literature indicates that descriptions of avian jaw anatomy are limited, with
45 studies of only a few species, use of two-dimensional drawings, and complicated written
46 descriptions. A major obstacle is the use of differing terminology (Holliday & Witmer 2007).
47 Papers that incorporate higher levels of detail include Lautenschlager, Bright and Rayfield's
48 description of the common buzzard jaw musculature (2013), Holliday and Witmer's description
49 and illustration of the albatross jaw musculature (2007), Elzanowski's description of the tinamous
50 jaw (1987), Zusi and Storer's pied-billed grebe jaw study (1969), Richards and Bock's
51 comparison of Hawaiian honeycreeper feeding apparatus (1973), and Zweers' description of
52 mallard myography (1974). From these descriptions it is evident that avian jaw muscle anatomy
53 differs in relative and absolute size of the various muscles, and in the position and extent of
54 attachments. Consequently, we determined that the jaw musculature in kingfishers should not be
55 reconstructed on the basis of anatomical descriptions of other families.

56

57 The jaw muscles of several species of kingfisher (though not *Dacelo novaeguineae*) have been
58 described by Burton (1984); however his illustrations are difficult to interpret, with little
59 information identifying which part of the skull he is referring to in the figures. Burton's
60 description did, however, reveal several variations in muscle origin and insertion areas between
61 the kingfisher species he studied. This observation reinforced the need to document the
62 kookaburra anatomy independently.

63

64 The lack of detailed published data on the kookaburra jaw musculature meant that firsthand
65 anatomical information was required to accurately model the jaw system. This information was
66 obtained through the dissection of the head of an adult laughing kookaburra (*Dacelo
67 novaeguineae*). The kookaburra was CT scanned prior to dissection, and this scan data was used
68 in conjunction with the dissection information to create a three-dimensional computer model of
69 the skull and jaw muscles of *D. novaeguineae*.

70 **A 3D approach to anatomical description**
71 Anatomy is inherently three-dimensional, but traditional descriptions of anatomy use a
72 combination of text and 2D picture modes. New technologies in data collection, assembly,
73 visualisation and communication, are offering significant new opportunities for improving the
74 study, documentation and publication of anatomy, particularly given the proliferation of 3D
75 imaging capabilities.

76 The following description adopts and exemplifies a three-dimensional approach to displaying

77 anatomical systems through the use of (1) three-dimensional Adobe Portable Document Format

78 (3D PDF) figures, and (2) 3D-enabled web pages. The 3D PDF medium allows an interactive 3D

79 model to be inserted into an electronic document in PDF format, meaning that specialised

80 software is not required to view the model other than the freely available Adobe Reader (desktop

81 version), and permanently embedding the figure directly in the document file. This method of

82 interactive visualisation is becoming increasingly popular, with publications in biomedical

83 science (Kumar et al., 2009; Selvam et al., 2009), astrophysics (Barnes & Fluke 2008),

84 invertebrate (Baeumler et al., 2008; Neusser et al., 2009; Ziegler et al., 2008) and vertebrate

85 anatomy (de Bakker et al., 2012; Holliday et al., 2013; Ruthensteiner & Heß 2008;

86 Lautenschlager, Bright & Rayfield, 2013) and paleontology (Knoll et al., 2012; Lautenschlager

87 2013). In addition, free, open source software that provides a pathway for the generation of 3D

88 PDF figures, especially for use in science, is now available (Barnes et al., 2013).

89 The 3D meshes produced for the 3D PDF were also used to generate a model available for

90 viewing in web pages. Web-based 3D visualisation is becoming more common with the growing

91 number of browsers supporting accelerated 2D and 3D graphics, especially via the WebGL

92 standard (http://www.khronos.org/webgl); recent examples include applications in bioinformatics

93 (Pettit & Marioni 2013), neuroinformatics (Ginsburg et al., 2011), and surgical teaching (Birr et

94 al., 2013). Like 3D PDF, web-based 3D visualisation enables the interactive manipulation of a 3D

95 model without requiring specialised software other than a modern web browser.

96 Here we present a detailed description of the 3D osteology and jaw musculature of *D.*

97 *novaeguineae,* and provide a summary of the avian jaw muscle synonymies. We aimed to

98 demonstrate and exploit the potential of 3D viewing technology in the anatomical sciences by

99 producing a 3D model that shows the position of the kookaburra jaw muscles on the skull relative

100 to one another; the model can be rotated and superficial muscles hidden or made transparent to

101 allow better visualisation of the deeper anatomy. While the 3D model allows for a detailed

102 descriptive model in a single figure-frame, it is only available for viewing in digital format. For

103 this reason, still images suitable for 2D print media are also included.

Materials & Methods

Specimen

106 A fresh, deceased adult laughing kookaburra (*Dacelo novaeguineae*), obtained from Australia

107 Museum's Ornithological collection (specimen no. AM BF2162) was used in the following

108 description. This specimen had died in the care of wildlife rescuers as a result of an infection on

109 the right elbow, although the head and skull did not show any obvious pathologies and thus were

110 deemed to illustrate normative anatomy.

Data acquisition and processing

112 The kookaburra was scanned in a clinical computed tomography (CT) scanner (Toshiba Aquilion

113 64) at the Newcastle Calvary Mater Hospital, at 120kV, 75mA and using a slice thickness of
114 0.5mm. The resulting DICOM images were imported into MIMICS v11 (MATERIALISE,
115 Belgium) segmentation software, wherein the skull of the kookaburra was digitally separated
116 from the soft tissue by combining a scalar threshold with manual selection tools; the high density
117 of the bone compared to the surrounding soft tissue allowed for quick and simple segmentation of
118 the skull by applying a threshold based on the grey scale pixel values representative of the bone.
119 A 3D model of the cranium and mandible was then created from this segmentation. This digital
120 skull model provided a scaffold to illustrate the muscle attachment points and muscle geometry
121 determined in the dissection (Fig. 1).
122
123 Segmentation of the jaw muscles proved more difficult due to the small size of the muscles, the
124 low resolution of the scanner and the use of CT (without staining for contrast) rather than MRI.
125 While the soft tissue making up the kookaburra jaw muscles was visible in the CT scan data, and
126 the bellies of the larger muscles could be differentiated and separated using MIMICS
127 segmentation tools, the resolution of the scan was too low to accurately identify the smaller jaw
128 muscles and the muscle attachment sites. For this reason, the soft tissue CT scan data was used
129 alongside the dissection information to identify placement of the jaw muscles (Fig. 1 & Fig. 2).
130
131 The jaw muscles were dissected out beginning with the superficial layer. Each individual muscle
132 was described using drawings, photographs and notes to illustrate its position, direction and
133 attachment sites. Muscles of the hyoid and eye were not required for the biomechanical analysis
134 and were not included in this study. The completed notes on kookaburra muscle anatomy were
135 compared with previously published data on avian jaw musculature (Baumel 1993; Burton 1984;
136 Elzanowski 1987; Holliday & Witmer 2007; Zusi & Storer 1969) to determine the individual
137 names of the jaw muscles observed. Muscle nomenclature used was based on Holliday and
138 Witmer (2007) and Burton (1984). Osteological nomenclature (Fig. 3) was based on Baumel
139 (1993), Zusi and Storer (1969)and Ghetie et al., (1976).
140
141 In conjunction with the CT scan data of the specimen, the illustrated dissection notes were used
142 to digitally recreate a three dimensional representation of the kookaburra jaw musculature on the
143 specimen's skull model (Fig. 2). This model was created using the CT editing software MIMICS
144 to manually select areas of the CT image slices where the muscles were determined to occur. The
145 CT slices were then joined in MIMICS to create a 3D model of each muscle which were
146 individually exported as stereolithography (STL) format files.

147 **3D image production**
148 **PDF**
149 A total of 16 segmented surfaces (meshes) – the cranium, mandible, and 14 muscles – comprise
150 the segmented jaw anatomy. The cranium was the largest and most detailed surface, and was
151 remeshed and simplified in MeshLab version 1.3.2 (Visual Computing Lab – ISTI – CNR;
152 http://meshlab.sourceforge.net) using a "Quadric Edge Collapse Decimation" to reduce its facet
153 count from ~635,000 to ~100,000; this reduced the total model size without significant visible

154 degradation. The meshes were converted (using MeshLab) to the widely-used Alias Wavefront
155 ".OBJ" format and listed in a text file, one per line, with colon-separated fields for the part
156 (anatomical) name, a group code, the filename, and the desired part colour expressed as an (r,g,b)
157 triplet. The group code is used to assign parts to named components in a two-level hierarchy. The
158 text file describing the model was read by a small, custom 3D visualisation program written using
159 S2PLOT (Barnes et al., 2006), and the surfaces were loaded, coloured and displayed for
160 inspection. Names were applied to the different meshes, and the export capability in the recent
161 S2PLOT release version 3.2.1 (Barnes et al., 2013) was used to save the complete 3-d model to a
162 Product Representation Compact (PRC) format file.

163 Additional lines in the model description file were used to: define standard views of the anatomy
164 (left lateral, right lateral, anterior, posterior, dorsal and ventral); to select a basic lighting
165 environment (a headlamp) and background colour; and to define the component group names.
166 From the model description file, a custom views file suitable for PDF embedding was generated,
167 and JavaScript fragments to toggle the various component groups were generated. Following the
168 workflow in Barnes et al., (2013), the PRC model was embedded in a LaTeX-format document
169 (Lamport, *LaTeX: A Document Preparation System (2ⁿᵈ Edition)*, 1994) and compiled into a PDF
170 file with embedded 3D figure, incorporating the custom views file and JavaScript fragments and
171 the standard 3D JavaScript code, included with S2PLOT version 3.2.1, which implements
172 standard keystrokes such as cursor keys to rotate the model and the letter 'a' to toggle autospin
173 mode.

174 **Web-based Figure**
175 Our web-based figure is based on the JavaScript *three.js* (http://threejs.org), public domain
176 extensions to *three.js* (via http://learningthreejs.com), and E. Graether's *TrackballControls.js*
177 (http://egraether.com). *Three.js* provides a simple entry point to visualisation of 3D scientific data
178 on the Web by supporting the loading of several common 3D model data formats, and rendering
179 the 3D model using WebGL (http://khronos.org/webgl) where available, and otherwise the 2D
180 Javascript canvas API for devices with no WebGL support. The OBJLoader.js module provides a
181 ready-made importer for the ubiquitous Alias Wavefront OBJ format. Using these components,
182 we developed a custom JavaScript-based web page that reads the identical model description file
183 used for assembling the 3D PDF figure, and constructs a web-based 3D visualisation, coloured as
184 for the 3D PDF version, and offering the same capability to interactively rotate and zoom the
185 model, and to toggle the model components.

186 **Results**

187 **Musculoskeletal anatomy**

Depressor Muscles:

188

189 1. *M. depressor mandibulae* (mDM) has a fleshy origin on the squamosal region on the back of

190 the braincase, just posterior to the opening of the ear. It becomes thicker as it extends around the

191 jaw joint to insert over most of the posterior surface of the mandible articular bone (Fig. 4 g,h).

192

Temporal Muscles:

193

194 The external adductor complex – *M. adductor mandibulae externus* (mAME) – has three parts:

195 2. M. *adductor mandibulae externus profundus* (mAMEp) originates along the length of the

196 temporal fossa; the attachment extends from the sagittal midline of the cranium (Fig. 4 g,h,) to

197 the region just dorsal to the zygomatic process and along the posterior edge of the post orbital

198 process. *M. adductor mandibulae externus profundus* inserts onto the coronoid process of the

199 mandible posterior to the insertion of *M. pseudotemporalis superficialis* (Fig. 4 a,b,j).

200 3. *M. adductor mandibulae externus superficialis* (mAMEs) has a narrow origin located on the

201 lateral side of the zygomatic process. It extends down around the medial side of the jugal where it

202 fans out to insert widely and thinly over the dorso-lateral surface of the mandibular ramus (Fig. 4

203 a,b,j).

204

205 4. *M. adductor mandibulae externus rostralis temporalis post-orbital lobe* (mAMErt): This

206 muscle is thought to be a member of the adductor mandibulae externus group. Burton (Burton

207 1984) labels it '*M. adductor mandibulae externus rostralis post-orbital slip*' or '*lobe*' in his

208 illustrations but only briefly mentions it in the text. We can find no other literature that uses this

209 term, but we retain its use here in lieu of further information on its possible homology. This

210 muscle was found to have a fleshy origin on the anterior/medial side of the post-orbital process. It

211 inserts onto the coronid process of the manidble, anterior to the insertion of *M. adductor*

212 *mandibulae externus profundus* (Fig. 4 a,b,j). It is clearly separate to the other parts of the

213 external adductor complex (mAME).

214 5. *M. adductor mandibulae posterior* (mAMP) originates along the orbital process of the

215 quadrate and the quadrate body (Fig. 4 a,c,i,j). It inserts onto the dorsal side of the mandible,

216 immediately antero-medial to the jaw joint.

Pseudotemporalis (mPST) Muscles:

217

218 6. *M. pseudotemporalis superficialis* (mPSTs) has two sections (displayed here as one muscle).

219 The medial part originates on the laterosphenoid process on the posterior wall of the orbit (Fig. 4

220 a,c,i). The lateral part originates slightly higher in the depression lateral to the process. Both

221 sections insert onto the medial side of the mandible where they fan out to cover most of medial

222 fossa of the mandible, dorsal to the insertion of M. *pseudotemporalis profundus* (Fig. 4 i,j).

223   7. *M. pseudotemporalis profundus* (mPSTp) originates from the medial point of the quadrate
224   orbital process (Fig. 4, a, i). The medial section of the muscle is thick and fleshy, while that
225   lateral side consists of a thin sheet fanning out as it inserts over a large area on the ventral edge of
226   the medial fossa of the mandible (Figure 4 i, j).

227

228   **Pterygoid (PT) Muscles:**
229   8. *M. pterygoideus dorsalis medialis anterior* (mPTDma) originates along the entire length of the
230   medial ridge of the palatine and onto the lateral edge of the pterygoid bone. It inserts onto the
231   anterior end of the mandible's medial process (Fig. 4 d,e,f,n,).

232   9. *M. pterygoideus dorsalis medialis posterior* (mPTDmp) takes its origin along the medial side
233   of the pterygoid bone, beginning from the joint of the palatine and pterygoid and inserting onto
234   the anterior edge of the medial mandibular process (Fig. 4 d,e,n).

235   10. *M. pterygoideus dorsalis lateralis* (mPTDl) has a fleshy origin on the anterior-most portion of
236   the palatine and down onto the dorsal lateral surface of the palatine. This large muscle wraps
237   down and around to insert onto the ventral/medial side of the mandible (Fig. 4 d,e,f,k,m,n).

238   11. *M. pterygoideus ventralis medialis* (mPTVm) originates along the entire ventral surface of the
239   palatine. It extends over the ventral side of the pterygoid bone to insert onto the anterior surface
240   of the tip of the medial mandibular process (Figure 4 k,l,m).

241

242   The *M. pterygoidus ventralis lateralis* (mPTVl) muscle is formed from three parts:

243   12. *M. pterygoideus ventralis lateralis Part 1* (mPTVl pt1) is a large, flat, superficial muscle
244   lying most ventral to all others. It originates along the lateral ventral ridge of the palatine and
245   along the lateral side of the crest where the palatine meets the vomer by an aponeurotic sheet
246   extending anteriorly until it merges with the skin of the palate. Posteriorly this muscle becomes
247   thicker as it extends over the posterior end of the mandible to wrap around and insert onto the
248   lateral side of the mandible, posterior to the attachment of *M. adductor mandibulae externus*
249   *superficialis* (Fig. 4 a,b,j,k,l).

250

251   13. *M. pterygoideus ventralis lateralis Part 2* (mPTVl pt2) – this muscle and *M. pterygoideus*
252   *ventralis lateralis part 3* occur closely together and it is possible that they are different heads of
253   the same muscle. Part 2 attaches to the lateral point of the palatine. It then extends back to fan out
254   and attach over a reasonably large area on the ventral side of the entire medial mandibular
255   process (Fig. 4 k,l,m).

256   14. *M. pterygoideus ventralis lateralis Part 3* (mPTVl pt3) runs laterally adjacent to Part 2. It
257   originates along the dorsal edge of the palatine, lateral to the palatine attachment of *M.*
258   *pterygoideus dorsalis lateralis.* This muscle attaches to the ventral crest of the medial mandibular
259   process (Fig. 4 f,k,m).

3D visualisation

261 An interactive, 3D model of the jaw muscles described above is available as Figure 5 in the
262 Appendix.

Discussion

Methodological issues

265 With the increasing use of CT as a primary means of collecting anatomical data for use in 3D
266 modelling, it is important to note the limitations of this imaging modality. Whilst it is possible to
267 collect the data required for the 3D modelling of the bones from CT alone, our experience with
268 the specimen used in this study is that incorporating detailed muscle anatomy into a 3D model
269 requires a combination of CT imaging and dissection. In CT, contrast between bone and soft
270 tissue is high, which maximises the accuracy of segmentation protocols (both automatic
271 algorithms and manual image processing) for segmenting bones. However, in the absence of
272 fixing protocols (eg. iodine potassium iodide – 'Lugol's iodine'), contrast between muscles and
273 other soft tissues is low and it is difficult to identify individual muscle bellies on the basis of CT
274 data alone; both the perimysium and intermuscular septa are inconsistently visible. An additional
275 limitation is the comparatively low resolution of medical CT in imaging small animals; for the
276 scans used in this study, maximum pixel resolution in each slice was 0.337 mm, which is a
277 relatively large proportion of the maximum cranial diameter (44 mm), even for a large kingfisher
278 species such as the kookaburra. Without the opportunity to use dissection to augment the 3D
279 imaging of muscle anatomy we could not have produced the level of anatomical data presented
280 here.

281 Whilst small-animal CT scanners (maximum field of view ~100 mm) or micro-CT (~20 mm) can
282 deliver significantly higher resolution than clinical CT, these scanners are not as readily available
283 as clinical CT scanners and we were not able to utilise one at the time of this study. These higher
284 resolution CT scanners also cannot produce images that clearly differentiate muscle bellies
285 without first preparing the specimen with an iodine stain, and require much longer scan times
286 than a clinical CT.

287 It is possible that magnetic resonance imaging (MRI) can provide an alternative to dissection by
288 producing high resolution images of the soft tissue, however MRI is not able to image bone well.
289 A specimen can be both CT and MRI scanned and the resulting images co-registered to fit to the
290 same 3D space co-ordinates, so that CT can be used to model the skeletal elements, while MRI
291 can provide muscle detail. At the time of this study an MRI scanner and co-registration code was
292 not available to us.

Nomenclature

294 Determining the correct names of particular muscles identified in the kookaburra based on
295 previous avian jaw anatomy literature was a complicated process. For many taxonomic groups,
296 anatomical descriptions have ranged across decades, languages, and authors; the issues we
297 discovered with respect to non-standard nomenclature are not restricted to kingfishers. Muscle
298 groups, particularly the *M. adductor mandibulae externus* and *M. pterygoideus dorsalis* muscles
299 were separated into several sections in some studies (Burton 1984; Richards & Bock 1973), or
300 treated as a whole in others (Holliday & Witmer 2007). Within this study, questions remain
301 regarding the extent to which some muscle bellies should be regarded as individual muscles, or
302 be considered as a part of a larger muscle. Specifically, is *M. adductor mandibulae externus*
303 *rostralis temporalis post-orbital* lobe part of one of the other *M. adductor mandibulae externus*
304 muscles (with the only reference found of a separate muscle in this area recorded by Burton
305 (1984); and should *M. pterygoideus ventralis lateralis Part 2* and *Part 3* be considered as
306 separate muscles to *M. pterygoideus ventralis lateralis Part 1*?

307

308 Nomenclature used in this study was based mainly on Burton's (1984) study as it includes
309 kingfisher anatomy and uses similar terminology to Baumel's Nomina Anatomica Avium (1993).
310 However, temporal muscle nomenclature was based upon Holliday and Witmer (2007). Baumel
311 (1993) and Burton (1984) each separate *M. adductor mandibulae externus* into three parts of
312 mAME rostralis, mAME ventralis and mAME caudalis, but we found no clear evidence of 5
313 separate heads for this muscle in *D. novaeguineae*. Holliday and Witmer's nomenclature for the
314 external adductor complex was more similar to the anatomy visible in our specimen.

315

316 There is a lack of consistency in the way in which muscle names are written and abbreviated in
317 text of previous literature. In an attempt to develop a standardised format for writing muscle
318 names and abbreviations, we use the following format:
   1. When writing the muscle name in text, we use an uppercase 'M.' (contraction for
       Musculus) at the start of the name, following Baumel's Nomina Anatomica Avium (1993).
   2. When writing the muscle name in full within text, we italicise the name; hence, *M.*
       pseudotemporalis superficialis. The muscle name is more easily distinguished visually
       from the surrounding text, making the text easier to read.
   3. When abbreviating the muscle (e.g. for figure labels), we use lower case for the 'm' and
       upper case for the abbreviation of the muscle name; hence, mPST. This format visually
       highlights the informative part of the label.
   4. Parts of the muscle are written in lower case, hence mPSTs and mPSTp. This makes it
       easier to identify the muscle under discussion, avoiding the potential confusion that can
       arise between muscles in the external adductor complex if the abbreviation for the part is
       written in upper case – Holliday and Witmer (2007) use mAMEP and mAMP for the *M.*
       adductor mandibulae externus profundus and the *M. adductor externus posterior*
       respectively. We abbreviate these muscles as mAMEp and mAMP.

333 Table 1 lists the avian jaw muscle nomenclature that we have used in this paper, the respective
334 abbreviations for use in labels, and the synonymies in selected literature. Note that some of these

335 published nomenclatures were presented as anatomical illustrations rather than written
336 descriptions, making it difficult to accurately determine exact muscle synonymy.

337 **The role of 3D images in communicating anatomical information**
338 Descriptive anatomy is the foundation for understanding functional anatomy. The recent surge in
339 biomechanical studies of form-function questions in a range of taxa means descriptive anatomy
340 remains as relevant as ever (Holliday et al., 2013). The current emphasis on 3D modelling
341 approaches indicates that anatomical data should be collated and communicated in 3D, as much
342 as is practically possible. It is certainly possible to communicate anatomical information to the
343 level required for 3D models using text or 2D diagrams; the issue is simply that a great deal of
344 text and/or a large number of 2D images are required. Conversely, a single 3D PDF figure or web
345 visualisation can communicate an equivalent level of information with the user being able to
346 interact with the model to gain finer understanding of structure.

347 **Acknowledgements**

348 The authors would like to thank; Phillip Clausen, Michael Mahony, Stephen Wroe, John Rodger,
349 Walter Boles, Jaynia Sladek, Australia Museum, Eleanor Cunningham, Newcastle Calvary Mater
350 Hospital

351 **References**

352 Baeumler N, Haszprunar G, and Ruthensteiner B. 2008. 3D interactive microanatomy of
353   *Omalogyra atomus* (Philippi,1841)(Gastropoda). *Zoosymposia* 1:101–118.
354 Barnes DG, and Fluke CJ. 2008. Incorporating interactive three-dimensional graphics in
355   astronomy research papers. *New Astronomy* 13:599-605.
356 Barnes DG, Fluke CJ, Bourke PD, and Parry OT. 2006. An Advanced, Three-Dimensional
357   Plotting Library for Astronomy. *Publications of the Astronomical Society of Australia*
358   23:82-93.
359 Barnes DG, Vidiassov M, Ruthensteiner B, Fluke CJ, Quayle MR, and McHenry CR. 2013.
360   Embedding and Publishing Interactive, 3-Dimensional, Scientific Figures in Portable
361   Document Format (PDF) Files. *PloS one* 8:e69446.
362 Baumel JJ. 1993. Handbook of avian anatomy: Nomina Anatomica Avium. *Publications of the*
363   *Nuttall Ornithological Club*.
364 Birr S, Monch J, Sommerfeld D, Preim U, and Preim B. 2013. The LiverAnatomyExplorer: A
365   WebGL-Based Surgical Teaching Tool. *Computer Graphics and Applications, IEEE*
366   33:48-58.
367 Burton PJK. 1984. Anatomy and evolution of the feeding apparatus in the avian orders
368   Coraciiformes and Piciformes. *Bull of the British Museum (Natural History Zoology ser)*
369   47.
370 de Bakker BS, de Jong KH, Hagoort J, Oostra R-J, and Moorman AFM. 2012. Towards a 3-
371   dimensional atlas of the developing human embryo: The Amsterdam experience.
372   *Reproductive Toxicology* 34:225-236.

373 Elzanowski A. 1987. Cranial and eyelid muscles and ligaments of the tinamous (Aves:
374   Tinaformes). *Zoologische Jahrbücher Abteilung für Anatomie und Ontogenie der Tiere*
375   116:63-118.
376 Ferrara T, Clausen P, Huber D, McHenry C, Peddemors V, and Wroe S. 2011. Mechanics of
377   biting in great white and sandtiger sharks. *Journal of Biomechanics* 44:430-435.
378 Ghetie V, Chitescu S, Cotofan V, and Hillebrand A. 1976. *Atlas de Anatomie a Pasarilor*
379   *Domestice*: Editura Academiei Republicii Socialiste Romania.
380 Ginsburg D, Gerhard S, Calle JEC, and Pienaar R. 2011. Realtime Visualization of the
381   Connectome in the Browser using WebGL. *Front Neuroinform Conference Abstract: 4th*
382   *INCF Congress of Neuroinformatics*.
383 Herrel A, O'Reilly J, and Richmond A. 2002. Evolution of bite performance in turtles. *Journal of*
384   *Evolutionary Biology* 15:1083-1094.
385 Herring SW, Rafferty KL, Liu ZJ, and Marshall CD. 2001. Jaw muscles and the skull in
386   mammals: the biomechanics of mastication. *Comparative Biochemistry and Physiology*
387   *Part A: Molecular & Integrative Physiology* 131:207-219.
388 Holliday CM, Tsai HP, Skiljan RJ, George ID, and Pathan S. 2013. A 3D Interactive Model and
389   Atlas of the Jaw Musculature of *Alligator mississippiensis*. *PloS one* 8:e62806.
390 Holliday CM, and Witmer LM. 2007. Archosaur adductor chamber evolution: integration of
391   musculoskeletal and topological criteria in jaw muscle homology. *Journal of Morphology*
392   268:457-484.
393 Knoll F, Witmer LM, Ortega F, Ridgely RC, and Schwarz-Wings D. 2012. The braincase of the
394   basal sauropod dinosaur *Spinophorosaurus* and 3D reconstructions of the cranial
395   endocast and inner ear. *PloS one* 7:e30060.
396 Kumar P, Vahedi-Faridi A, Saenger W, Merino E, de Castro JAL, Uchanska-Ziegler B, and
397   Ziegler A. 2009. Structural basis for T cell alloreactivity among three HLA-B14 and HLA-
398   B27 antigens. *Journal of Biological Chemistry* 284:29784-29797.
399 Lauder GV, Huey RB, Monson RK, and Jensen RJ. 1995. Systematics and the study of
400   organismal form and function. *BioScience* 45:696-704.
401 Lautenschlager S. 2013. Palaeontology in the third dimension: a comprehensive guide for the
402   integration of three-dimensional content in publications. *Paläontologische Zeitschrift*:1-
403   11.
404 Lautenschlager S, Bright JA and Rayfield EJ. 2013. Digital dissection – using contrast-enhanced
405   computed tomography scanning to elucidate hard- and soft-tissue anatomy in the
406   Common Buzzard *Buteo buteo*. Journal of Anatomy
407 Neusser TP, Heß M, and Schrödl M. 2009. Tiny but complex-interactive 3D visualization of the
408   interstitial acochlidian gastropod *Pseudunela cornuta* (Challis, 1970). *Frontiers in*
409   *zoology* 6:20.
410 Pettit J, and Marioni J. 2013. BioWeb3D: an online webGL 3D data visualisation tool. *BMC*
411   *Bioinformatics* 14:185.
412 Quayle MR. 2011. A Morphological Study of the Kingfisher Skull. Environmental Science and
413   Management Honours Thesis, University of Newcastle.
414 Richards LP, and Bock WJ. 1973. Functional anatomy and adaptive evolution of the feeding
415   apparatus in the Hawaiian honeycreeper genus *Loxops* (Drepanididae). *Ornithological*
416   *Monographs*:i-173.
417 Russell E. 1916. Form and Function. A Contribution to the History of Animal Morphology. J.
418   Murray. London (Reprint Chicago University Press 1982).
419 Ruthensteiner B, and Heß M. 2008. Embedding 3D models of biological specimens in PDF
420   publications. *Microscopy research and technique* 71:778-786.
421 Selvam L, Vasilyev V, and Wang F. 2009. Methylation of zebularine: a quantum mechanical
422   study incorporating interactive 3D pdf graphs. *The Journal of Physical Chemistry B*
423   113:11496-11504.
424 Thompson DAW. 1916. On Growth and Form. Cambridge University Press.

425 Wroe S, McHenry C, and Thomason J. 2005. Bite club: comparative bite force in big biting
426   mammals and the prediction of predatory behaviour in fossil taxa. *Proceedings of the*
427   *Royal Society B: Biological Sciences* 272:619-625.
428 Ziegler A, Faber C, Mueller S, and Bartolomaeus T. 2008. Systematic comparison and
429   reconstruction of sea urchin (Echinoidea) internal anatomy: a novel approach using
430   magnetic resonance imaging. *BMC Biology* 6:33.
431 Zusi RL, and Storer RW. 1969. Osteology and myology of the head and neck of the pied-billed
432   grebes (Podilymbus). *University of Michigan Miscellaneous Publications of the Museum*
433   *of Zoology* 139:1-49.
434 Zweers GA. 1974. Structure, movement, and myography of the feeding apparatus of the mallard
435   (*Anas platyrhynchos L*.) A study in functional anatomy. *Netherlands Journal of Zoology*
436   24:323-467.

Figure 1

Segmentation of the CT data

The CT scan data for the *Dacelo novaeguineae* head was imported into the segmentation software MIMICS (MATERIALISE, Belgium) (a). The skull was segmented out using thresholding tools to select the regions of bone from the scan images, while the muscles were manually segmented. Segmentation is indicated by the coloured regions on the CT image. The segmented regions on each CT image slice were then joined using Mimics modelling tools to create a 3D model of the *D. novaeguineae* skull and jaw muscles (b). The red line through the skull in (b) indicates the location of the CT slice in (a). Jaw muscles shown in this model are 1. *M. depressor mandibulae*, 2. *M. adductor mandibulae externus profundus*, 3. *M. adductor mandibulae externus superficialis*, 4. *M. adductor mandibulae externus rostralis temporalis post-orbital lobe*, 5. *M. adductor mandibulae posterior*, 6. *M. pseudotemporalis superficialis*, 7. *M. pseudotemporalis profundus*, 8. *M. pterygoideus dorsalis medialis anterior*, 9. *M. pterygoideus dorsalis medialis posterior*, 10. *M. pterygoideus dorsalis lateralis*, 11. *M. pterygoideus ventralis medialis*, 12. *M. pterygoideus ventralis lateralis Part 1*, 13. *M. pterygoideus ventralis lateralis Part 2* and 14. *M. pterygoideus ventralis lateralis Part 3*.
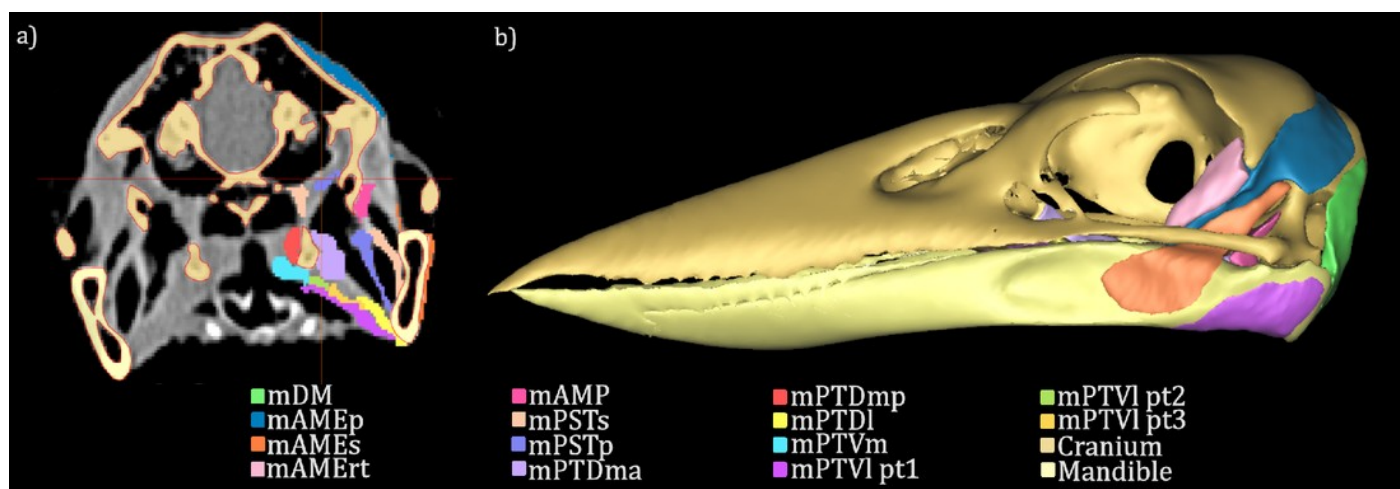
Figure 2

Comparing the dissection to the digital model

Each of the jaw muscles of the laughing kookaburra (*Dacelo novaeguineae*) were individually described and removed during the dissection (a). Notes, drawings and photographs from the dissection were used to identify the jaw muscles on the CT scan so that they could be digitally segmented and modelled (b). This diagram shows the placement of the muscles in the dissected specimen (a) and their digital representation (b). Muscle shown here are 1. *M. depressor mandibulae*, 2. *M. adductor mandibulae externus profundus*, 3. *M. adductor mandibulae externus superficialis*, 4. *M. adductor mandibulae externus rostralis temporalis post-orbital lobe* and 12. *M. pterygoideus ventralis lateralis part 1* (removed in dissection photo).
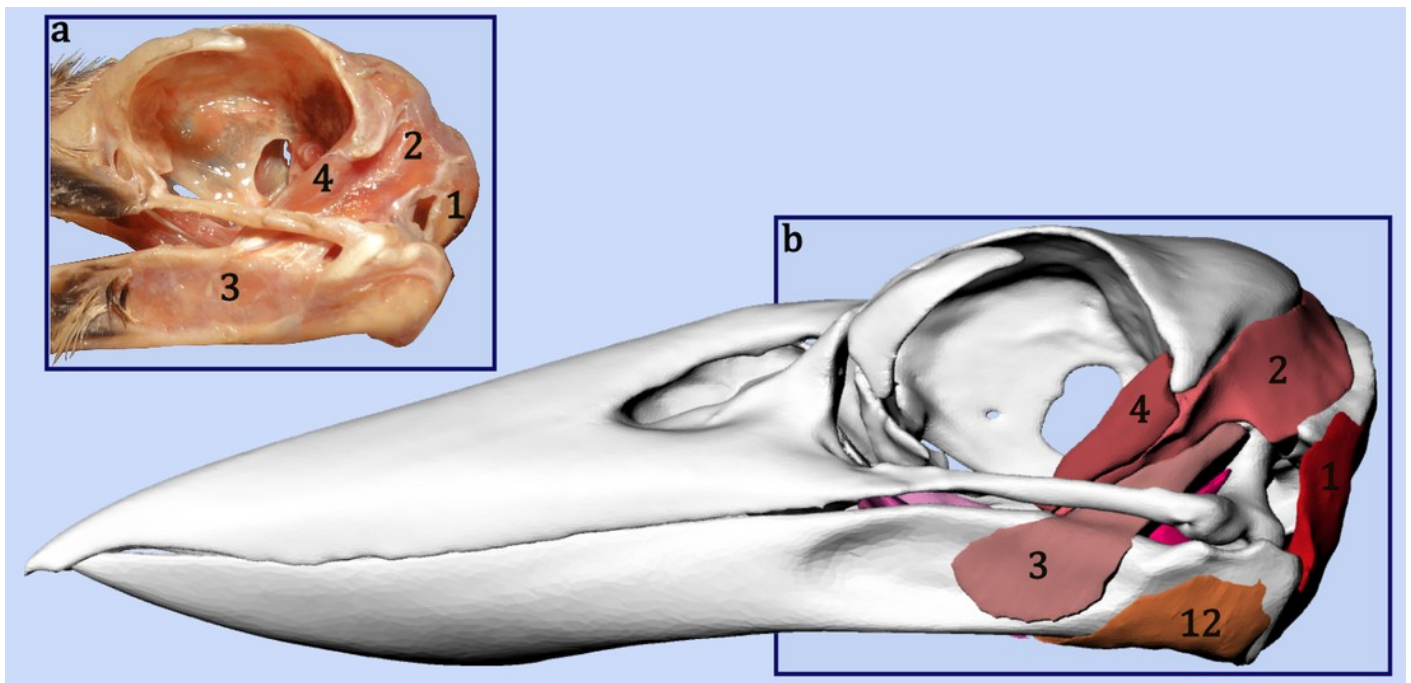
Figure 3

Osteology of the avian skull

Illustrating the bones and features of the avian skull on *Dacelo novaeguineae* in a) anterior, b) posterior, c) lateral, d) dorsal and e) ventral views. f) shows the features of the mandible in dorso-lateral view. Due to the fused nature of avian skull bones, the separation between the bones is not defined. Adapted from (Baumel 1993; Ghetie et al. 1976; Zusi & Storer 1969)
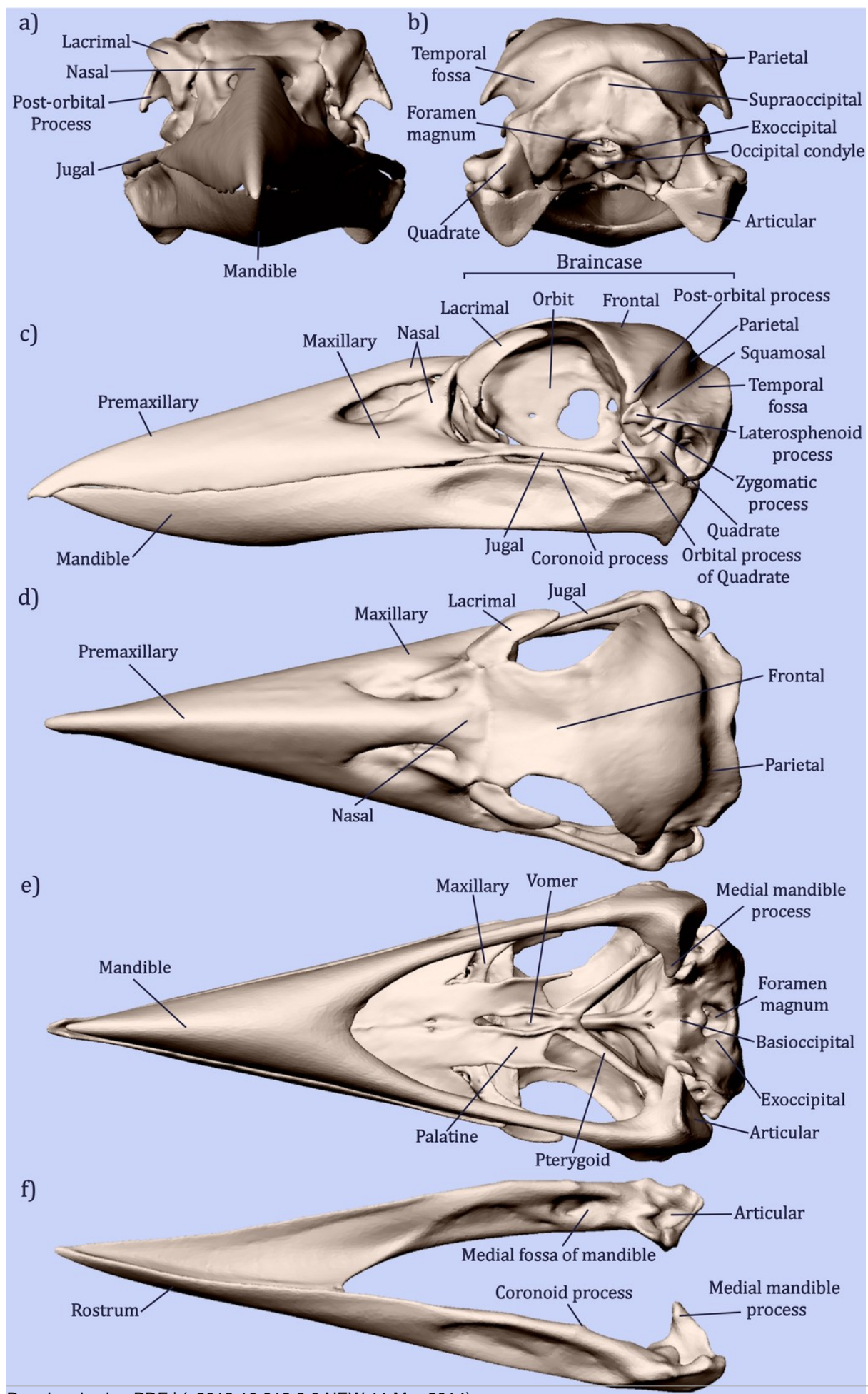
Figure 4

Jaw musculature of the Australian Laughing Kookaburra *Dacelo novaeguineae*

a) Lateral view showing the attachment areas of the jaw muscles, b) the geometry of the jaw muscles and c) deeper muscle geometry with muscle 2,3 and 4 hidden. d) Showing the geometry of the *M. pterygoideus dorsalis* muscles and e) their position in a transparent skull. f) Dorsal view of a transparent skull showing attachment sites of the *M. pterygoideus* muscles to the dorsal side of the palatine and pterygoid bones. g) Attachment sites of muscles on the posterior side of the skull and h) their geometry. i) geometry of the *M. adductor mandibulae externus* and *M. pseudotemporalis* muscles, skull is shown with a transparent mandible to display their medial attachment to the mandible. j) Dorsolateral view of the muscle attachment sites on the mandible. k) Muscle attachment sites on the ventral side of the skull, and the geometry of l) superficial, m) middle and n)deep layers of ventral muscles. 1. *M. depressor mandibulae*, 2. *M. adductor mandibulae externus profundus*, 3. *M. adductor mandibulae externus superficialis*, 4. *M. adductor mandibulae externus rostralis temporalis post-orbital lobe*, 5. *M. adductor mandibulae posterior*, 6. *M. pseudotemporalis superficialis*, 7. *M. pseudotemporalis profundus*, 8. *M. pterygoideus dorsalis medialis anterior*, 9. *M. pterygoideus dorsalis medialis posterior*, 10. *M. pterygoideus dorsalis lateralis*, 11. *M. pterygoideus ventralis medialis*, 12. *M. pterygoideus ventralis lateralis Part 1*, 13. *M. pterygoideus ventralis lateralis Part 2* and 14. *M. pterygoideus ventralis lateralis Part 3*.
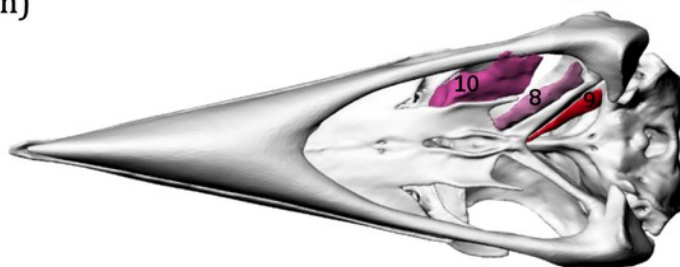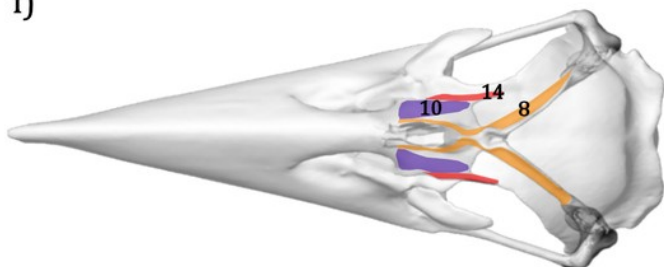
Table 1_(on next page)

Jaw muscle nomenclature

Equivalent avian jaw muscle names used in this study and selected literature. Muscle equivalents of which we are uncertain are designated by (?).

This study:	This study abbreviation:	Baumel (1993)	Ghetie et al. (1976)	Burton (1984)	Richards & Bock (1973)	Holliday & Witmer (2007)
1. M. depressor mandibulae	mDM	M. depressor mandibulae	M. occipitomandibularis	M. depressor mandibulae	M. depressor mandibulae a,b and c	Not included
2. M. adductor mandibulae externus profundus	mAMEp	M. adductor mandibulae externus rostralis temporalis	M. temporalis	M. adductor mandibulae externus rostralis temporalis	M. adductor mandibulae externus rostralis temporalis	M. adductor mandibulae externus profundus
3. M. adductor mandibulae externus superficialis	mAMEs	M. adductor mandibulae externus rostralis	M. masseter superficialis (?)	M. adductor mandibulae externus rostralis lateralis	M. adductor mandibulae externus rostralis lateralis	M. adductor mandibulae externus superficialis
4. M. adductor mandibulae externus rostralis temporalis post-orbital lobe	mAMErt	Part of M. adductor mandibulae externus rostralis (?)	M. masseter	M. adductor mandibulae externus rostralis temporalis post-orbital lobe	Part of M. adductor mandibulae externus rostralis temporalis (?)	Part of M. pseudotemporalis superficialis or M. adductor mandibulae externus profundus (?)
5. M. adductor mandibulae posterior	mAMP	M. adductor mandibulae externus profundus caudalis	M. quadratomandibularis superficialis	M. adductor mandibulae externus caudalis	M. adductor mandibulae posterior	M. adductor mandibulae posterior
6. M. pseudotemporalis superficialis	mPSTs	M. pseudotemporalis superficialis	M. mandibularis infraorbitalis (?)	M. pseudotemporalis superficialis	M. pseudotemporalis superficialis	M. pseudotemporalis superficialis
7. M. pseudotemporalis profundus	mPSTp	M. pseudotemporalis profundus	M. quadratomandibularis profundus oralis	M. pseudotemporalis profundus	M. pseudotemporalis profundus	M. pseudotemporalis profundus
8. M. pterygoideus dorsalis medialis anterior	mPTDma	M. pterygoideus dorsalis medialis	M. pterygomandibularis (?)	M. pterygoideus dorsalis medialis	M. pterygoideus dorsalis medialis anterior	M. pterygoideus dorsalis
9. M. pterygoideus dorsalis medialis posterior	mPTDmp	M. pterygoideus dorsalis medialis	M. craniopterygoquadratus oralis (?)	M. pterygoideus dorsalis medialis	M. pterygoideus dorsalis medialis posterior	M. pterygoideus dorsalis
10. M.	mPTDl	M.	M.	M.	M.	M.

This study:	This study abbreviation:	Baumel (1993)	Ghetie et al. (1976)	Burton (1984)	Richards & Bock (1973)	Holliday & Witmer (2007)
pterygoideus dorsalis lateralis		pterygoideus dorsalis lateralis	mandibulopalatinus pars lateralis	pterygoideus dorsalis lateralis	pterygoideus dorsalis lateralis	pterygoideus dorsalis
11. M. pterygoideus ventralis medialis	mPTVm	M. pterygoideus ventralis medialis	M. mandibulopalatinus pars medialis	M. pterygoideus ventralis medialis	M. pterygoideus ventralis medialis	M. pterygoideus ventralis
12. M. pterygoideus ventralis lateralis part 1	mPTVl pt1	M. pterygoideus ventralis lateralis	Not determined	M. pterygoideus ventralis lateralis	M. pterygoideus ventralis lateralis	M. pterygoideus ventralis
13. M. pterygoideus ventralis lateralis part 2	mPTVl pt2	M. pterygoideus ventralis lateralis	Part of M. mandibulopalatinus pars medialis (?)	M. pterygoideus ventralis lateralis	M. pterygoideus ventralis medialis fan	M. pterygoideus ventralis
14. M. pterygoideus ventralis lateralis part 3	mPTVl pt3	M. pterygoideus ventralis lateralis	M. entotympanicus (?)	M. pterygoideus ventralis lateralis	Not determined	M. pterygoideus ventralis

3D visualisation of skull bones and jaw musculature in *Dacelo novaeguineae*

This 3D figure is an appendix to Quayle et al., "An Interactive Three Dimensional approach to Anatomical Description - The jaw musculature of the Australian Laughing Kookaburra (*Dacelo novaeguineae*)." If viewing from within Adobe Reader, click on the image to activate the 3D model. To use the model, click to view the label for each structure, left click and drag to free rotate, control left click and drag to pan, use scroll wheel to zoom. Select the "Toggle Model Tree" icon to show/hide individual components of the model. Right click on the component names in the "Model Tree" to make transparent. Muscle labels: 1 mDM *M. depressor mandibulae*, 2 mAMEp *M. adductor mandibulae externus profundus*, 3 mAMEs *M. adductor mandibulae externus supercialis*, 4 mAMErt *M. adductor mandibulae externus rostralis temporalis post-orbital lobe*, 5 mAMP *M. adductor mandibulae posterior*, 6 mPSTs M. pseudotemporalis supercialis*, 7 mPSTp *M. pseudotemporalis profundus*, 8 mPTDma *M. pterygoideus dorsalis medialis anterior*, 9 mPTDmp *M. pterygoideus dorsalis medialis posterior*, 10 mPTDl *M. pterygoideus dorsalis lateralis*, 11 mPTVm *M. pterygoideus ventralis medialis*, 12 mPTVl pt1 *M. pterygoideus ventralis lateralis Part 1*, 13 mPTVl pt2 *M. pterygoideus ventralis lateralis Part 2* and 14 mPTVl pt3 *M. pterygoideus ventralis lateralis Part 3*.

Figure 5: 3D visualisation of skull bones and jaw musculature in *Dacelo novaeguineae*.
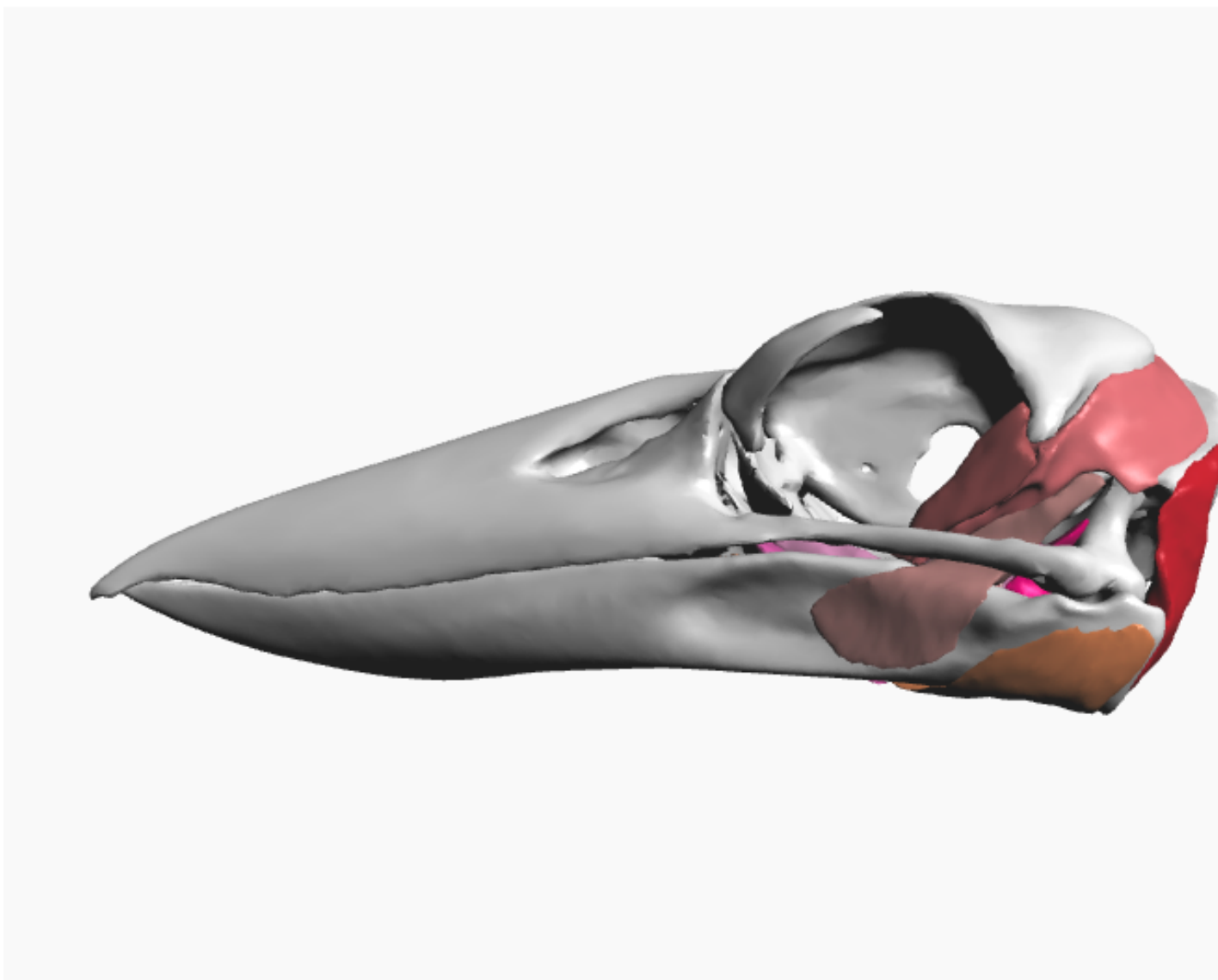
Object:

Toggle: Cranium; Mandible; Depressor muscle; Temporal muscles; Pseudotemporalis muscles; Dorsal Pterygoid muscles; Ventral Pterygoid muscles.

This 3D figure is an appendix to Quayle et al., "An Interactive Three Dimensional approach to Anatomical Description - The jaw musculature of the Australian Laughing Kookaburra (*Dacelo novaeguineae*)." If viewing from within Adobe Reader, click on the image to activate the 3D model. To use the model, click to view the label for each structure, left click and drag to free rotate, control left click and drag to pan, use scroll wheel to zoom. Select the "Toggle Model Tree" icon to show/hide individual components of the model. Right click on the component names in the "Model Tree" to make transparent. Muscle labels: 1 mDM *M. depressor mandibulae*, 2 mAMEp *M. adductor mandibulae externus profundus*, 3 mAMEs *M. adductor mandibulae externus superficialis*, 4 mAMErt *M. adductor mandibulae externus rostralis*, 5 mAMP *M. adductor mandibulae posterior*, 6 mPSTs *M. pseudotemporalis superficialis*, 7 mPSTp *M. pseudotemporalis profundus*, 8 mPTDma *M. pterygoideus dorsalis medialis anterior*, 9 mPTDmp *M. pterygoideus dorsalis medialis posterior*, 10 mPTDl *M. pterygoideus dorsalis lateralis*, 11 mPTVm *M. pterygoideus ventralis medialis*, 12 mPTVl pt1 *M. pterygoideus ventralis lateralis* Part 1, 13 mPTVl pt2 *M. pterygoideus ventralis lateralis* Part 2 and 14 mPTVl pt3 *M. pterygoideus ventralis lateralis* Part 3.